Journal of Materials Processing Tech. 255 (2018) 364–372

Contents lists available at ScienceDirect

Journal of Materials Processing Tech.

journal homepage: www.elsevier.com/locate/jmatprotec

Advancing electrochemical jet methods through manipulation of the angle of address

J. Mitchell-Smith, A. Speidel, A.T. Clare*

Advanced Component Engineering Laboratory (ACEL), Advanced Manufacturing Technology Group, University of Nottingham, Nottingham, NG7 2RD, United Kingdom

ARTICLE INFO

Keywords:
Electrochemical machining
Angle of address
EJM
Micro-milling
Nickel superalloy

ABSTRACT

Electrochemical jet processing techniques have traditionally been considered to be limited to planar interactions with the electrolyte jet being maintained normal to the workpiece surface. In this study, the viability and resultant effects of articulating the nozzle relative to the work were investigated for the first time. Two machining conventions were defined, normal, where the jet is maintained perpendicular to the traverse direction, and push/pull, where the nozzle is rotated with respect to the direction of travel. It was found, with the normal convention that a range of differing resultant profile surface geometries could be created; unique to this process. This was demonstrated by the changing resultant side wall slopes found through the rotation of the head with up to 80% difference between the slopes of the cut walls. The adjacent wall to the nozzle slope decreasing as the jet angle approaches 90° whilst the opposite side wall slope increases. Predictable ratios of the differing slopes of the striation side walls were then able to be defined. The push/pull convention demonstrated that deeper, sharper cuts are possible due to the highly localising current density effect of nozzle inclination achieving a 35% increase in depth without requiring additional energy. Also, that resultant surface finish could be greatly improved, reducing the profile roughness (R_a) from 0.2 µm in the pull mode to 0.04 µm in the push mode achieving a mirror-like finish. The mechanics of these phenomena are investigated and defined. The influence of nozzle jet speed variation combined with inclining the jet was also studied. This was found to have no noticeable influence on the resultant profile when the nozzle is inclined. In contrast, when the nozzle is normal to the surface, jet velocity is seen to have a direct influence due to polarisation effects relating to the poor clearance of machining debris and the formation of oxides. It is shown that through variation of the angle of jet address an extra level of flexibility and performance is possible within electrochemical jet processes.

1. Introduction

Electrochemical jet processing (EJP) is a manufacturing technology based on electrolysis and is the amalgamation of electrochemical jet machining (EJM) as described by Kunieda (1993) and electrochemical jet deposition (EJD) as reported by Bocking et al. (1995), within the same machine tool (Fig. 1). EJP in subtractive mode is capable of achieving mask-less, high precision material removal and has been previously demonstrated across a range of applications for structuring of component interface surfaces. Yang et al. (2016) applied EJP in subtractive mode for controlling droplet adhesion on superhydrophic surfaces. Enhanced cutting surfaces were developed by Kunieda et al. (2010). Surface Meso-scale structuring has been applied by the process in several advanced tribological applications such as roller bearings (Kunieda, 1993). In addition reducing wear rates in automotive applications have been explored including cylinder liners (Walker et al., 2017) and processing of hardened materials for transmissions components and forming tools (Schubert et al., 2011a,b). The latter further employing the process to create surface microstructures for enhanced heat removal (Schubert et al., 2011a,b). As demonstrated in these applications, EJP is traditionally considered a planar machining technique where the nozzle is maintained normal to the workpiece at all times (Fig. 1). Considerable research has been carried out into assessment of the effects of changing the angle of address in other applied energy beam processes. For instance Venkatesh (1984) investigated the optimum angle for increased depth of cut in abrasive water jet machining (AWJ). AWJ was also assessed for 3D milling through variation of the jet impingement angle by Srinivasu et al. (2009). Beam articulation has been of focus in laser processes, Tokarev et al. (1995) developed a self-limiting method for polishing of diamond films utilising changes in the beam angle of incidence. In comparison George et al. (2004) investigated the angular dependence of focused laser ablation with nanosecond pulses and the resultant geometry in polymers for the development of simulations for direct-write applications. However, to

* Corresponding author.
E-mail address: adam.clare@nottingham.ac.uk (A.T. Clare).

https://doi.org/10.1016/j.jmatprotec.2017.12.026
Received 9 September 2017; Received in revised form 12 December 2017; Accepted 17 December 2017
Available online 20 December 2017

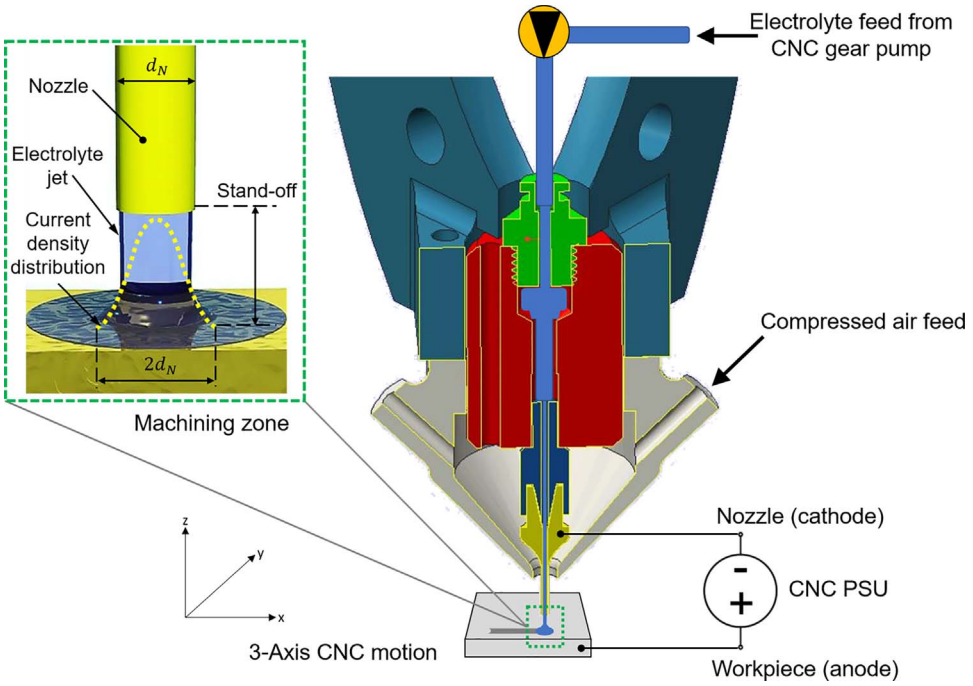

Fig. 1. Process schematic of EJP in subtractive configuration in the normal mode of operation whereby the jet is perpendicular to the work.

the authors' knowledge, no consideration has been given to the impact of altering the jet angle of address to the substrate surface in EJP. As indicated in prior research, consideration of jet approach angle is a key concern in industrial usage of all applied energy beam processes. Exploration of the effects and associated mechanics would enable a step change in the viability of EJP as an efficient micro-milling technology capable of producing complex 3D shapes.

EJP is distinct from other energy beam processes, in that the energy distribution is distinctly governed by electrical field effects with respect to the surface. This is unlike other energy beam processes whereby the energy density maxima is maintained in line of sight of the approaching beam regardless of surface considerations and the angle of address. This was again demonstrated by George et al. (2004) who found that ablation depth along the direction of the incident laser beam is independent of the angle of incidence in laser ablation. Srinivasu et al. (2009) observed the same phenomena in AWJ, whereby slope of the kerf trailing edge decreases with the lowering of the approach angle alongside the maximum kerf depth which remains in line with the jet axis (Fig. 2). It is therefore proposed that resultant profiles from EJP would not follow the same findings.

A common simplification for EJP modelling dictates that the energy distribution remains as a constant Gaussian distribution as defined by Yoneda and Kunieda (1995) in subtractive machining mode. The same being defined by Rajput et al. (2015) in deposition mode. This is regardless of the spatial influence of the changing inter-electrode gap (IEG) and traverse speed. Therefore, erroneous or indeed purposeful changes to the jet address have not yet been considered by researchers.

It is well recognised that the IEG in electrochemical machining (ECM) can be considered partially as a simplified resistor as proposed by Kozak et al. (2008) for pulse electrochemical micromachining. Furthermore, Kawanaka and Kunieda (2015) considered the same in electrolyte jet machining. Therefore, applying Ohms law to a typical jet arrangement (Eq. (1)):

$$V = IR = \pi \frac{{d_N}^2}{4} JR \tag{1}$$

Where V is voltage (V), I, current (A), R resistance (Ω), d_N the diameter of the nozzle (mm) and J being current density (A/cm^2). If current is constant and voltage allowed to float, regardless of variation in resistance (resulting from variation in the size of the IEG), constant applied current density will be maintained and as such material removal will remain constant. This is true when considering the IEG on the macro-scale.

As the nozzle is rotated away from the normal, the tip contour is no longer parallel to the work surface. Since resistance is dependent on spatial considerations of discrete areas between electrodes (Eq. (2)) (Mitchell-Smith et al., 2017), it is proposed that localised in-jet resistance across the impingement area becomes dependant on the shortest current pathway at a specific point.

$$R = \frac{l}{A} \rho_E \tag{2}$$

Where ρ_E is the resistivity of the electrolyte. This in turn is hypothesised to lead to a change in the shape of the resultant machined profile as the peak energy distribution is shifted.

A multitude of approaches in generating 3D structures have been previously employed in planer subtractive EJP techniques. Superimposition of toolpaths were demonstrated in research by Natsu et al. (2007). The variation of process parameters to effect profile changes has also been investigated (Hackert-Oschätzchen et al., 2012). This is accompanied by contributions which investigate combinations of machining strategies (Schubert et al., 2016). These demonstrate complex approaches to the generation of surface structures, whereby the articulation of the jet in two further axis may remove the need for this complexity.

The purpose of this work is to explore the effects which occur as a result of variation in the incident jet angle. This will comprise of not only geometrical changes in the resultant profile but also finish when using two distinct machining conventions. Furthermore, this work intends to identify the fundamental mechanisms which effect material removal and further implementation of EJP.

2. Methodology

A previously developed CNC EJP platform described by Mitchell-Smith et al. (2014), was utilised in subtractive mode coupled to a new end effector (Fig. 3). This enables a head that can be manually set at varying indexed angles to alter the impingement angle of the jet against the workpiece (θ = 22.5°, 45°, 67.5°, 90°, 112.5°, 135°, 157.5°). An axial air shroud was incorporated to reduce undesirable machining

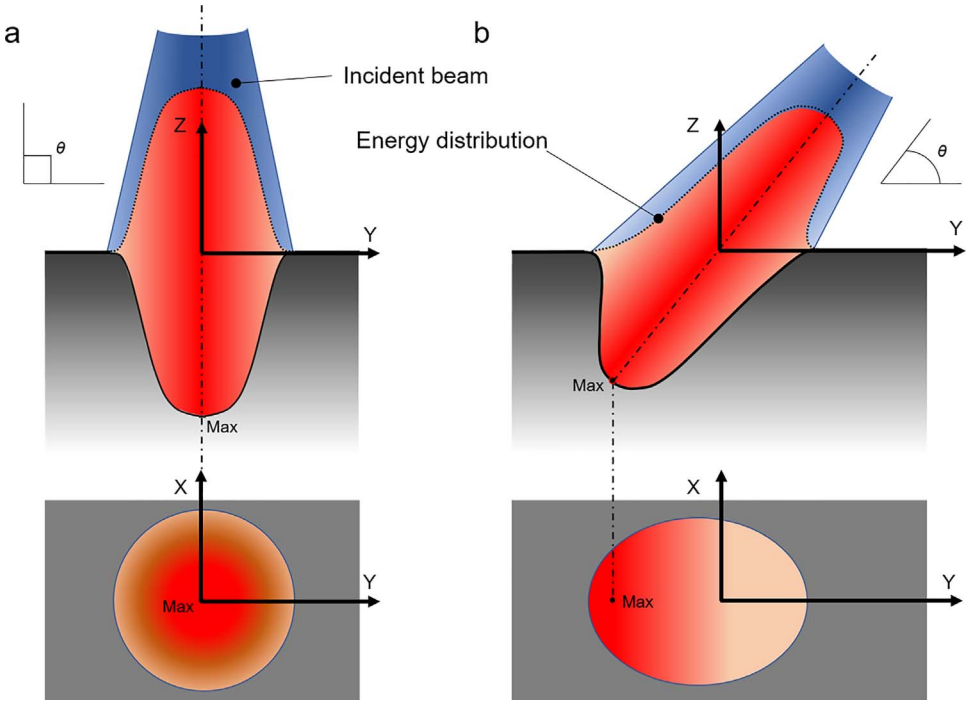

Fig. 2. Schematic of removal profile effect based on abrasive waterjet (Srinivasu et al., 2009), whereby the maximum energy density is maintained in line of sight of the beam address regardless of the approach angle (a) angle of address normal to the workpiece surface, (b) reduced angle of address.

affects (Hackert et al., 2008) and aid restriction of the dissolution area.

2.1. Influence of angle of address

During experiments some process parameters remained constant. The electrolyte ($NaNO_3$, 2.3 M) was maintained at 22 °C, and supplied using a 500 µm internal diameter (I.D.) stainless-steel nozzle. Stand-off was set by an automatic touch-sense system (Mitchell-Smith and Clare, 2016) at 250 µm from the nearest nozzle edge to the workpiece. Current was maintained at 410 mA ($J = 200$ A/cm^2) and electrolyte flow rate at 0.27 l/min ($V_{jet} = 23$ m/s) with a traverse feed of 0.5 mm/min throughout. Compressed air was fed to the air shroud at 4 bar. Single pass striations were repeated across a nickel superalloy (Inconel 718) workpiece at each θ value. Inconel 718 was chosen for prior knowledge in processing parameters and its difficulty to be processed efficiently by traditional means.

The striations were machined in both directions across the workpiece with what is referred to in this instance as the "normal" convention (Fig. 4a). This is defined as the nozzle being maintained perpendicular to the traverse direction of the head, with the head being articulated in the Y direction through each θ angle. Secondly, repeated striations were machined with the nozzle being translated axially to the traverse direction of the head (Fig. 4b) again through all θ angles giving rise to a "push/pull" convention where the nozzle tip can be seen to

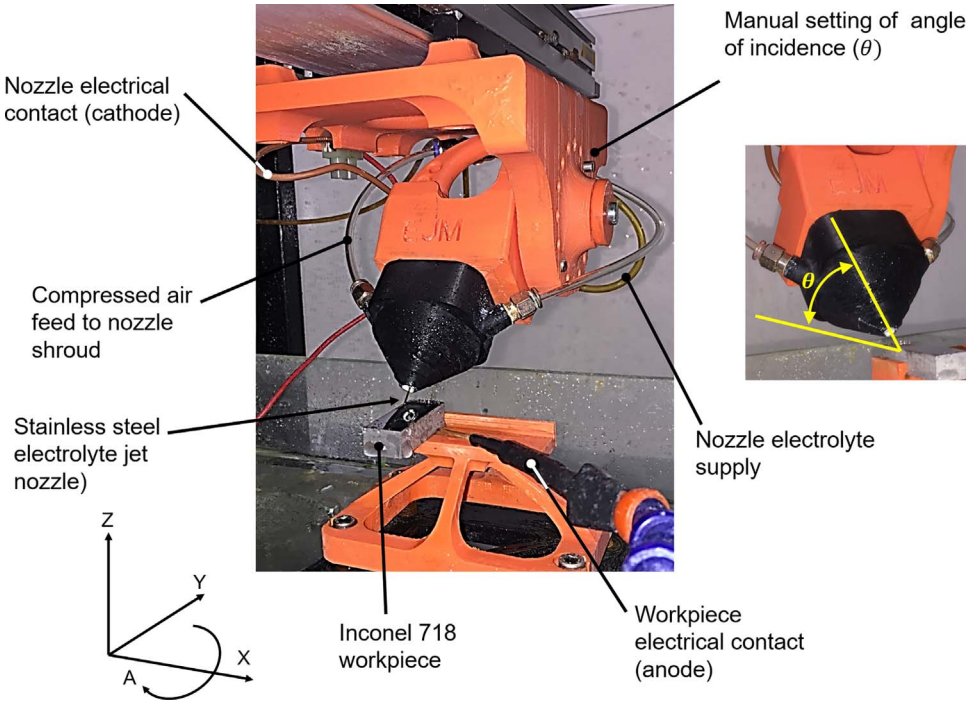

Fig. 3. Apparatus used to create the varying incident jet angles noting the global co-ordinates system used throughout.

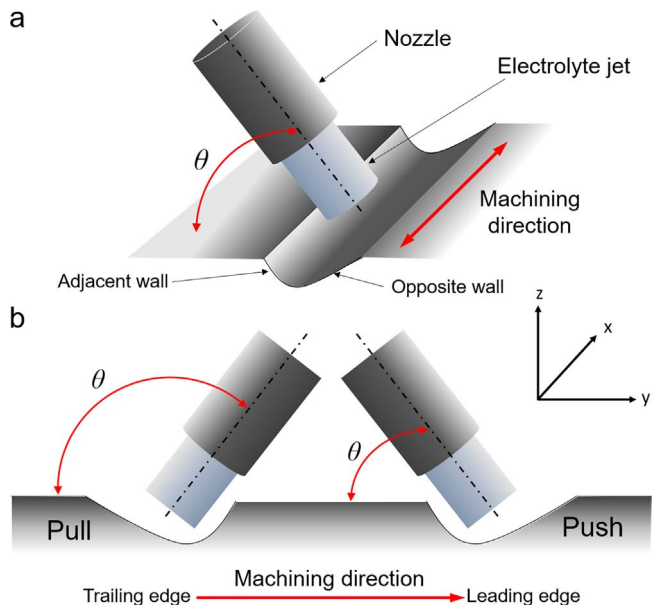

Fig. 4. Schematic of machining approach convention (a) being of normal convention and (b) being push-pull convention.

push or pull the electrolyte jet.

The resulting machined striations were scanned using a non-contact, focus variation microscope, Alicona G5 Infinite Focus. Using Digital Surf Mountainsmap software, the generated surface maps were analysed to quantitatively assess the slopes of the cut walls, area of the material removed and depth/width of the resultant profile. Standard deviation (SD) is taken as the maximum value of dispersion from the mean value within a sample data set, presented as a percentage of the mean value. The resultant surface textures from the push/pull machining convention were analysed using SEM (Philips XL 30), as these are seen to be similar to the 'climbing' phenomena observed in conventional milling operations. In this case, it can be described as push mode (climb) and pull mode (conventional). Profile roughness (R_a) was also extracted through the software and filtered in accordance to ISO 16610-21 (2011). Multiple lines were extracted from the base of the cut profile and up to 1/3rd of each side noting the Gaussian current density distribution means this area has the highest energy density as perceived at the surface. This was carried out to ascertain if there is any advantage to adopting a particular strategy.

2.2. Influence of jet speed variation

In order to ascertain the influence of jet ejection on the response profile, a secondary set of experiments was devised. Repeated striations were carried out with the head indexed at 22.5° and 67.5° using the predefined normal machining convention. For each angle, the jet speed of the impinging electrolyte was varied through 3 steps, 4 m/s, 14 m/s and 29 m/s covering the complete capability of the machine. The resultant profiles were then compared to those previously obtained to geometrically assess for any variation in the resultant profile attributable to variation in jet speed.

3. Results and discussion

3.1. Normal convention

Considering the resultant profiles of initial experiments (examples of which can be seen in Fig. 5), the profile is shown to be dependent primarily upon approach angle and as dissimilar to that found in any other beam type process shown in Fig. 2.

It can be considered as opposite to that found in comparable processes whereby the peak in energy is maintained in line of sight of the axial centre line of the approaching beam regardless of approach. Therefore, the slope of the adjacent edge would be of a shallower slope as the angle of incidence lessens and the opposite wall would become steeper and in some processes even create an under-cut. This is the reverse of the findings reported here.

The cross-sectional area of the profiles exhibit little variation achieving a mean area of 18,323 μm^2 with a maximum deviation of 3.5% across all angles of address. The depth and width of the striations show variation throughout the different approach angles. The width being the mean taken from 22° sample profiles and 157.5° profiles is 1219 μm (SD 2.4%) compared to the width at 90° being 1031 μm (SD 1.4%). The maximum depth also shows a reduction from 41 μm (SD < 1%) measured as the mean depth of 22° sample profiles and 157.5° profiles to 33 μm (SD < 1%) for the jet normal to the surface. This demonstrates that there is no change in the dissolution mechanism as the area removed is unaffected, so in agreement with Faraday's law the applied energy per unit volume material removed remains constant. However, the profile geometry is unequivocally affected by the approach angle with the profile displaying an asymmetrical appearance.

Considering Fig. 6, it is demonstrated that the resultant profiles achieve a high degree of symmetry about the 90° position. The adjacent walls at 22.5° and 157.5° having a variation of 2.2% (368 μm/mm–360 μm/mm) between the mean slope values and 5.6% variation between the opposite walls (68 μm/mm to 73 μm/mm). The total deviation of the adjacent walls being 7% between opposing angle pairs and 2.3% for the opposite wall of opposing angle pairs. The profile created at 90° shows a 3% variation between the slopes of the cut walls. The variation in symmetry is attributed to assembly tolerances leading to reduced precision when indexing the head as allied work reported by the author with Walker et al. (2017), where angle of address is not varied, the deviation seen here is not present.

The overall trend can be clearly seen in Fig. 6. The adjacent slope decreasing as the jet angle approaches 90° whilst the opposite angle increases. The reverse occurring beyond 90°.

Taking the mean of the cut walls for the pair 22.5° and 157.5° the adjacent wall has a ratio of 5:1 times steeper than the opposite wall. This ratio then reduces to 4.5:1 for the 45°/135° pair and 2.2:1 for the slope of adjacent to opposite ratio for the 67.5°/112.5° pair. The 90° angle having a ≈1:1 ratio.

The reason for this trend being different to that found in other jetting techniques can be understood by consideration of Fig. 7. The 2D schematic describes the two main influencing factors; changing localised resistance in the IEG due to the changing nozzle angle, therefore the distance to the surface at discrete points and secondly the spatial changes due to the nature of the electrolyte jet itself causing a confluence of current pathways. The air around the jet acting as a dielectric to confine the current paths to the jet. With the nozzle, perpendicular to the surface, the current density distribution is understood to be Gaussian (Yoneda and Kunieda, 1995) with equal resistance across the nozzle tip as described by Mitchell-Smith et al. (2017). Using discrete, arbitrary points A, B and C on the workpiece surface, Fig. 7 highlights the mechanics attributed to the creation of the asymmetrical profiles. Fig. 7a shows the nozzle addressed at 67.5° with no electrolyte jet present. Point *C* on the nozzle tip is now closer to the surface so will provide the lowest resistance point and therefore a preferential current pathway leading to enhanced material removal at this point. However, the spacing of the primary current paths, which are the most direct path from surface to nozzle tip remain constant.

In Fig. 7b the electrolyte jet is superimposed to the electrostatic scenario. Here we can see the spacing between the primary current paths has changed due to the jet bringing point C closer to point B at the work surface. This is at the expense of the current pathway becoming longer so less preferential at point A. The secondary current paths with less influence on the overall machined shape can also now be seen to be more confined and centred about the B / C zone. Considering the

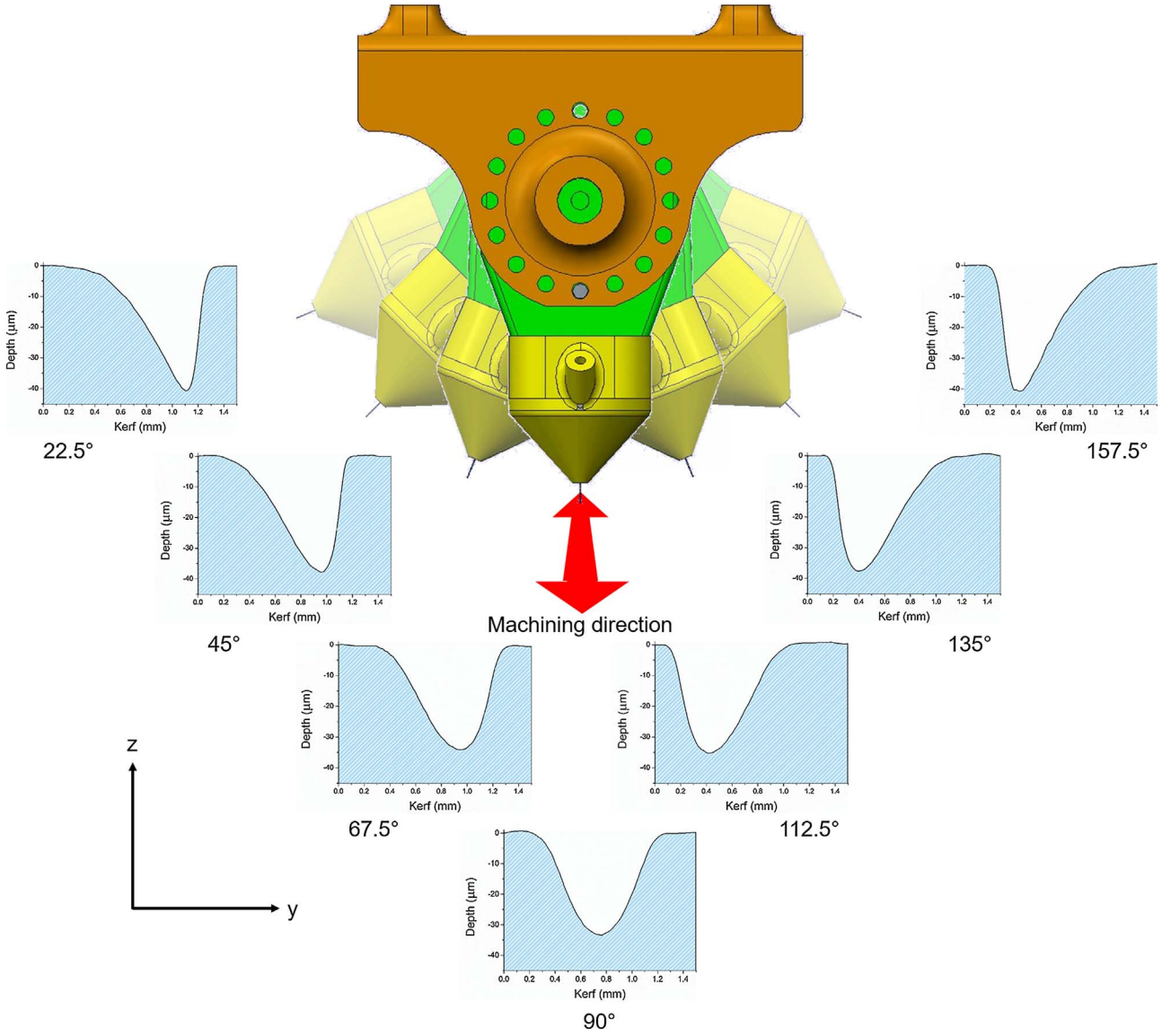

Fig. 5. Example profiles taken from striations created with the angled head using the normal convention.

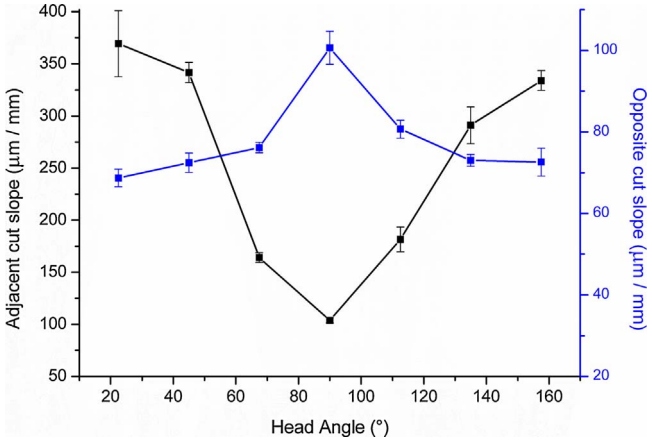

Fig. 6. Comparison of the adjacent and opposite striation wall slopes through the range of angles of address.

example profile in Fig. 5 for 67.5°, the slight shift to the right for the deepest point, therefore maximum current density corresponding to this, can clearly be seen. Fig. 7c, shown without the jet, continues to show the exaggerated trend. The resistance at point C is now significantly reduced in comparison to any other point on the nozzle tip surface.

The spacing of the primary current pathways is reduced making it more concentrated, there is no preferential area of dissolution as they still maintain an even spacing. Noting at this point that the secondary current paths are spread away from the nozzle. Considering Fig. 7d, with the electrolyte jet incorporated, all primary current paths across the nozzle now converge at a single point, that being the path of least resistance. Only secondary current pathways spread across the footprint. Observing the resultant profile from Fig. 5 for 22.5° the maximum depth that is achieved corresponding to the peak in applied energy is seen at the extreme right of the profile. At this angle, it is also possible that electrolyte ejection effects from the cut could affect the slope of opposite wall elongating the intersection with the un-machined surface where little current is expected to flow.

At this point it can be proposed that the distribution of the current density field takes on an inverse Gaussian distribution where the peak of the current density is shifted from the centre of the cut in line with the rotation of the nozzle.

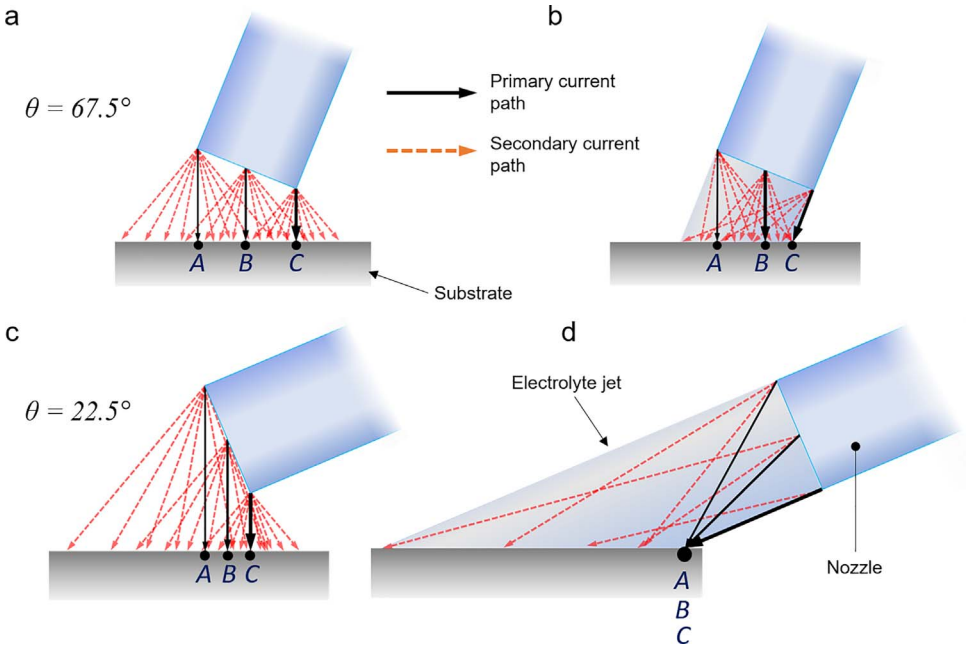

Fig. 7. Schematic of varying current pathways as a function of nozzle and jet angle. Points A, B and C are discrete arbitrary points located on the surface under the nozzle. Fig. 7a and c showing the preferential pathways of the primary and secondary current paths with an inclined nozzle. Fig. 7b and d showing the further influence the electrolyte jet has at re-directing and converging these pathways leading to an asymmetrical machined profile.

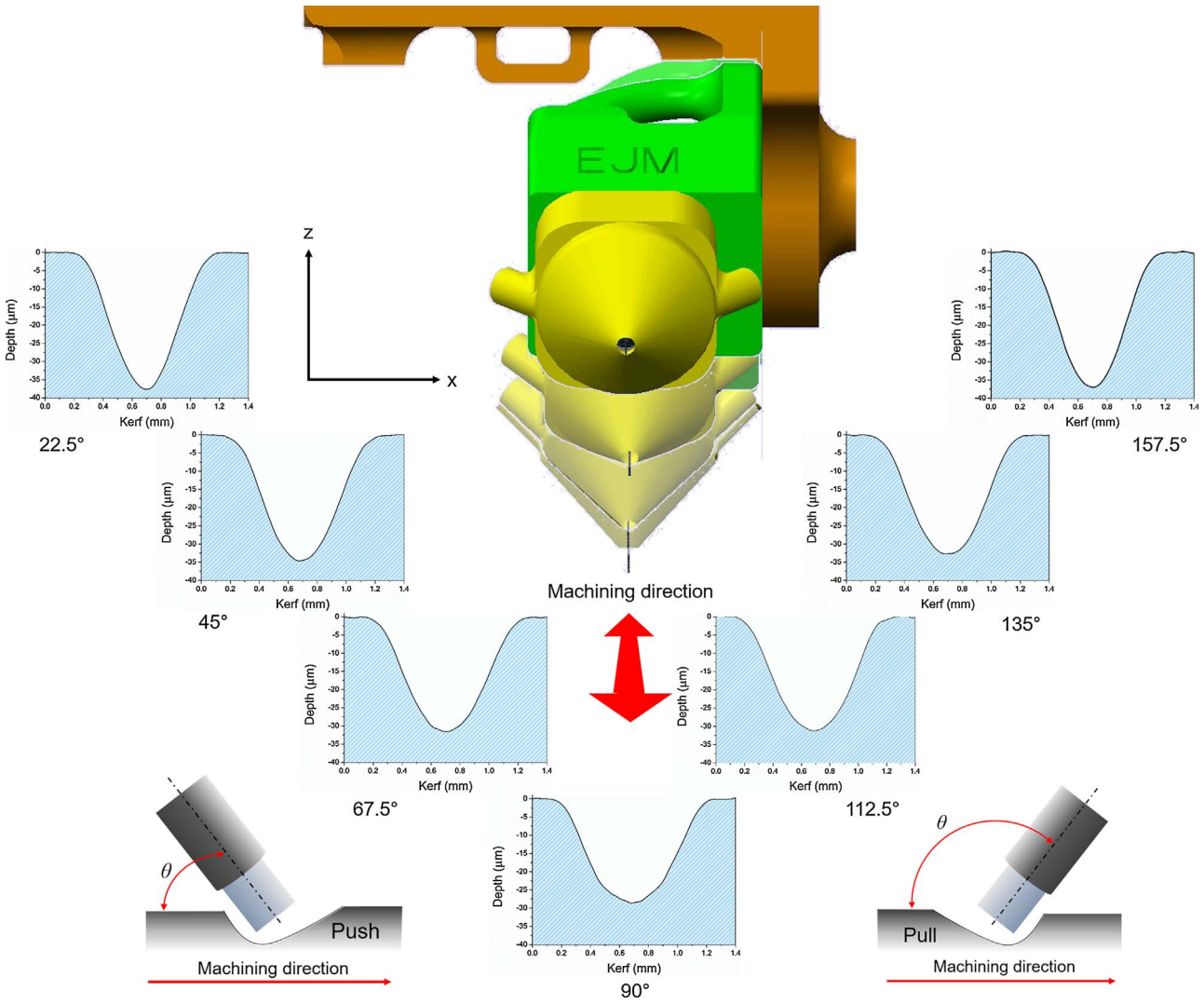

Fig. 8. Examples of profiles taken using the push/pull convention.

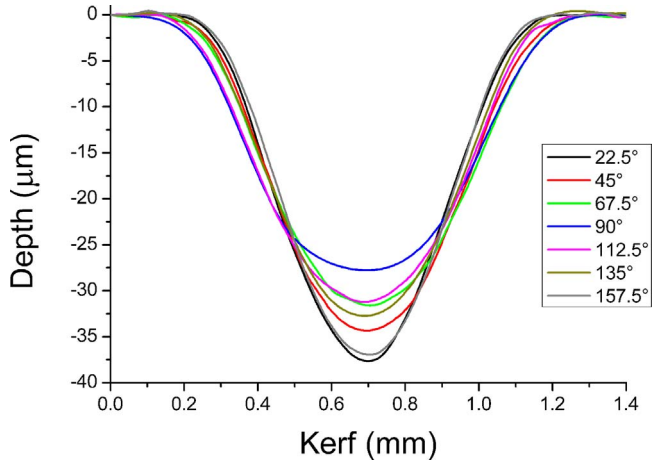

Fig. 9. Example profiles from push/pull convention overlaid to demonstrate changing energy distribution through different approach angles.

3.2. Push/pull convention

The resultant profiles using the push/pull convention (examples of which can be seen in Fig. 8) do not demonstrate the same changes in symmetry as seen with the normal convention with profiles remaining symmetrical throughout. The mean variation across all the sample striations from the left-hand slope to the right-hand slope being 1.1%. The resultant profile area again shows little variation with a mean area across all sampled profiles of 18,608 µm^2 (1.5% difference to the mean area from the normal convention) with a maximum deviation of 1.5%.

There are however, changes to the profile geometry. The same trend in depth change from the normal convention is seen in push/pull modes. Taking the mean depths from the samples of 22° and 157.5° giving 37.7 µm depth (SD 1%) compares to the depth at 90° approach of 28 µm (SD 1.6%). The side walls show a reduction in slope from the steepest side walls at 22.5°/157.5° being 123 µm/mm (SD 4%) to 104 µm/mm (SD 2.6%) at 45°/135° and 95 µm/mm (SD 3.5%) for the angle pair 67.5° / 112.5°.

The differences can be observed in Fig. 9, where all the profiles are overlaid on the same axis. The conflux effect seen in the normal convention profile is mimicked in the push/pull profiles. Higher angles of address having a deeper, narrower profile with a sharper apex compared to the profile with the jet being perpendicular, causing a wider, shallower more rounded distribution of energy. This is due to the equilibrium distance of all points around the nozzle contour and less confluence nature of the jet as previously noted in the normal convention.

The change in current density distribution is due directly to the angle of approach. This is further supported when the resultant surface finish is considered from the push / pull experiments seen in Fig. 10.

In the push mode of Fig. 10a, (θ = 22.5°) surface roughness is shown to be significantly lower when compared to the pull mode of operation. This is obvious, not only in the surface scans but also in the accompanying SEM (Fig. 10). This results in a mean R_a across all samples of 0.04 µm (SD 10%) achieving a high lustre, reflective, appearance corresponding with a near mirror finish as defined by Prakash and Struik (1981) and in EJM by Kawanaka and Kunieda (2015). When the nozzle is at 90° associated with the traditional approach (Fig. 10b) the resultant finish is markedly different with preferential etching of grain boundaries and the largely nickel matrix, leading to a high degree of precipitate "wash out" (Speidel et al., 2016). This "preferential" machining regime results in a much higher roughness leading to an R_a of 0.14 µm (SD 4.2%). Fig. 10c demonstrates the resultant finish obtained when in the pull mode (θ = 157.5°).

Although the form of the profile mirrors that found at 22.5° meaning the same applied current, the surface can be seen to have undergone a more "sporadic" dissolution effect whereby the breakdown of oxide layers and debris removal is unequal across the surface leading to uneven dissolution and a higher roughness in comparison to the two previous modes with an R_a of 0.2 µm (SD 10%).

These surface texturing effects are commonly associated with the level of current density as observed at the surface, in line with observations by Kawanaka et al. (2014). Consideration of Fig. 11 highlights that the trailing edge of the jet dominates the final surface finish. In push mode (Fig. 11a) the energy density at the trailing edge is seen to be at the maximum therefore leading to the smoothest finish. In comparison, at the other extreme in pull mode (Fig. 11c), the IEG is at its largest at the trailing edge, therefore, the energy level is at the lowest

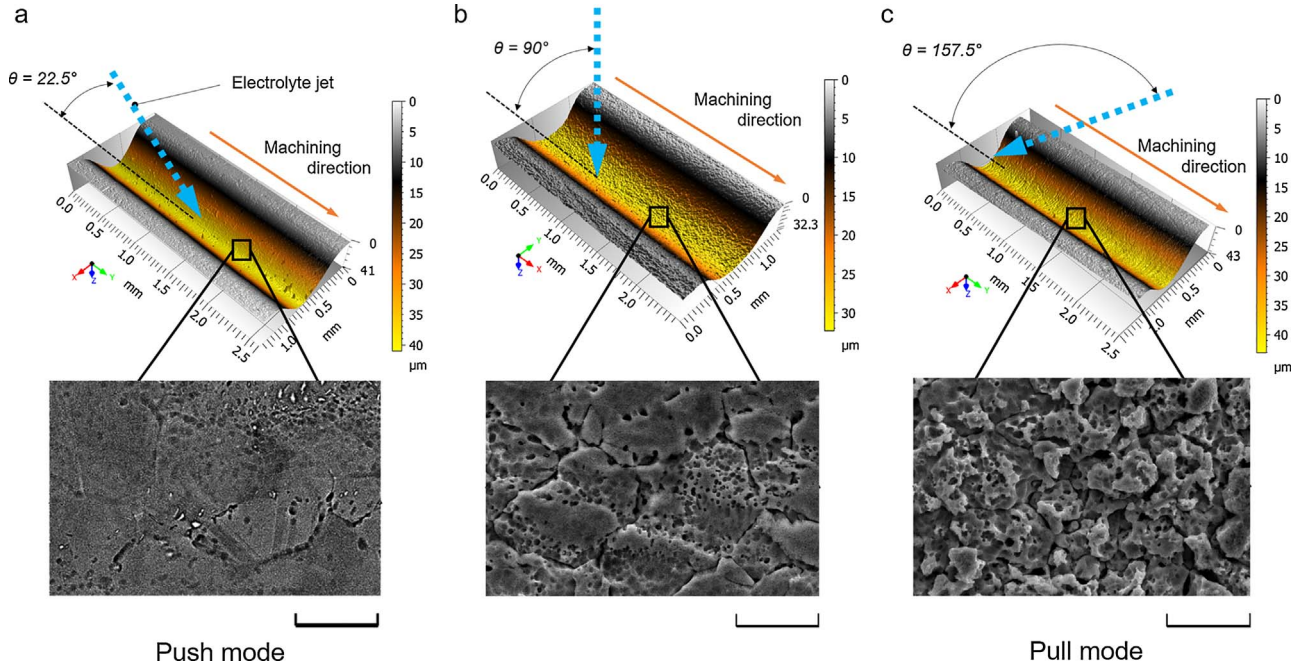

Fig. 10. Extracted example surfaces and SEM micrographs of resultant surface (7.5k× Magnification, all scale bars are 10 µm) from cuts at 22.5° (a), 90° (b) and 157.5° (c).

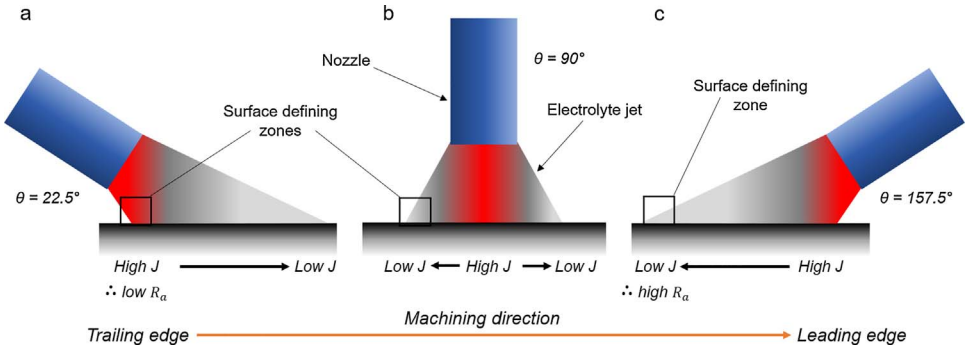

Fig. 11. Schematic of energy distribution affecting surface finish (a) push mode (b) normal mode (c) pull mode.

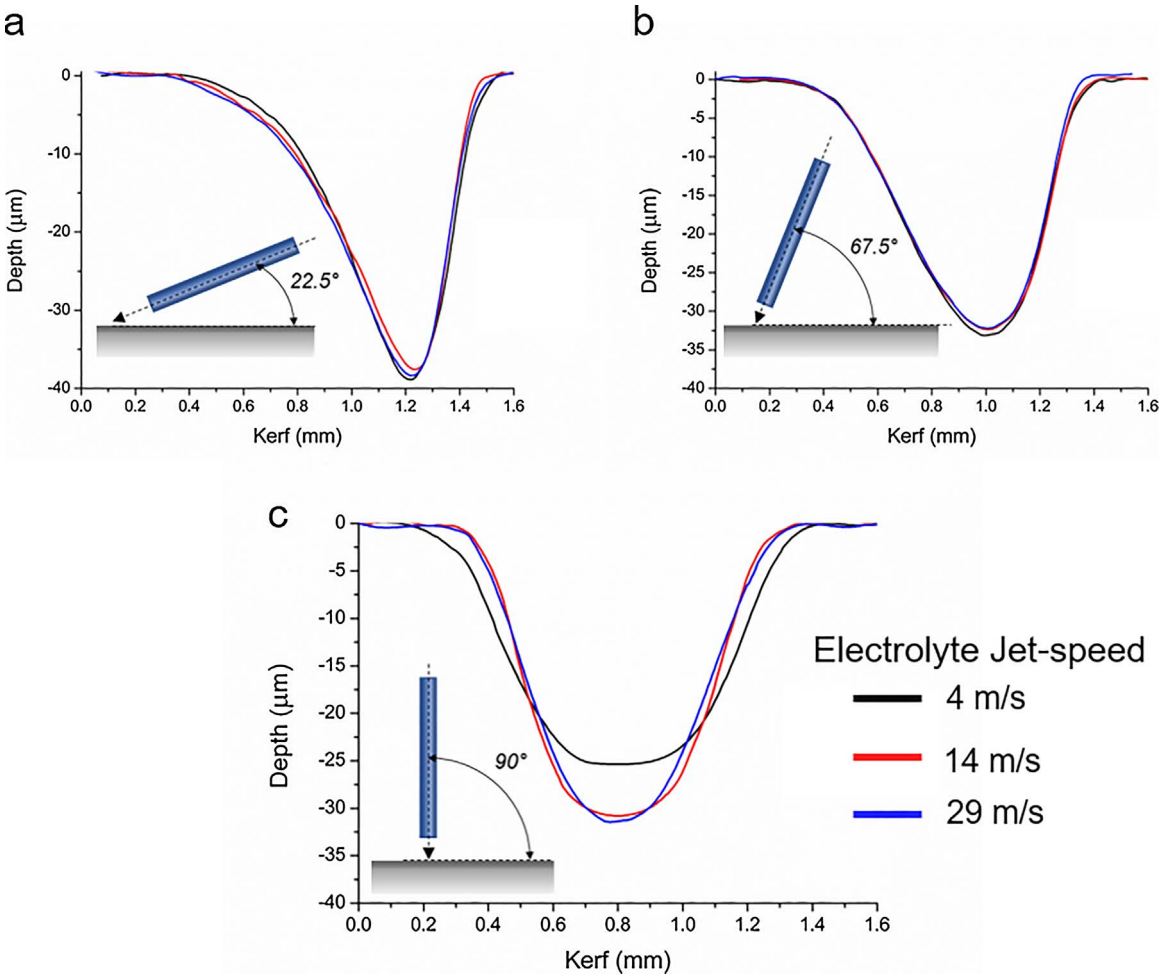

Fig. 12. Impact of varying electrolyte jet speed on resultant profile. (a) with the nozzle inclined at 22.5°, (b) 67.5° and (c) 90° to the workpiece surface noting the invariance of depth at tilted regimes.

leading to a low energy dissolution regime. The normal mode although having the trailing edge in the lowest area of current density the IEG is considerably smaller than that at the trailing edge of the pull mode. Therefore, as resistance is directly related to the gap between electrodes and resistance is inversely proportional to current so, the smaller IEG at that point in the normal mode means a higher current transfer is possible. This is demonstrated by the lower surface roughness of the normal mode than the pull mode.

3.3. The effect of jet velocity on the resultant profile

Fig. 12 shows the resultant profiles created when the nozzle is angled at 22.5°, 67.5° and 90° to the workpiece surface and the jet-speed varied through 4 m/s, 14 m/s and 29 m/s covering the range possible with pump used in this apparatus.

It should be noted that achieving precision machining at the lowest jet speeds demonstrated here is only possible due to the use of the nozzle air shroud which creates a thin film area reported with higher jet velocities, where a hydraulic jump is observed at the periphery of a thin film (Kai et al., 2012). Observed in Fig. 12a and b there is little impact on the resultant profile within the range tested here. The created profile also mimics those profiles found earlier in Section 3.1 with the lower angles achieving greater depth due to the higher localised current density. Both sets of striations demonstrate a mean profile area of 18,493 µm^2 and a standard deviation of 1.7% across all samples which is less than 1% difference from the profiles created earlier, showing

there is no noticeable impact of varying jet speed. This further demonstrates the mechanisms of current transfer dominating the resultant profile rather than any ejection effects. The variation seen in Fig. 12c of the depth reduction of 19% (SD < 1%) at the lowest jet speed compared to the highest speed and increase in kerf width, has been previously observed by Mitchell-Smith et al. (2017). This is explained by the increasing jet speed enabling clearing of debris and localised oxidisation within the cut, leading to a reduction in current flow to the surface directly below the jet. Interestingly, this phenomenon is not encountered when the nozzle is inclined. This may be due to the ejection of debris and other polarising artefacts from the IEG having a facilitated route. While in the normal mode a stagnation point will occur in the jet centre and inhibit debris ejection.

4. Conclusions

It was clearly demonstrated that the jet approach angle in EJP has a direct effect on the resultant machined form and finish.

Through simple articulation of the incident jet it is possible to locally modulate in-jet resistance therefore distorting the energy distribution perceived at the work surface.

This was demonstrated by changing resultant side wall slopes found through the rotation of the head with an 80% difference between the slopes of the cut walls at 22.5°/157.5° angle pair to 3% difference at a 90° approach. The steepest wall was always found to be where the smallest IEG was created nearest to the nozzle tip.

It was also demonstrated by the resultant surface finish found in the push and pull modes where the position of the trailing edge of the jet dominates the surface finish created. In the push mode where the nozzle was angled at 22.5°, the trailing edge was shown to receive the highest current density therefore resulting in a surface finish (R_a) of 0.04 µm. In comparison, the surface finish in pull mode had a surface finish (R_a) of 0.2 µm where the trailing edge is shown to be dominated by low current density. This demonstrates that surface finish can be controlled by the angle of address.

Further to this, the use of the angle pair 22.5°/157.5° using both normal and push/pull conventions gives a ≈23% increase in depth when compared to the address at 90°. This is due to a confluence of current pathways produced due to the nature of the electrolyte jet approach and the restricted contour of the nozzle tip addressing the surface.

Jet velocity was not found to have an impact within this study, on the geometry created when the nozzle approach is inclined and the electrolyte jet speed varied. This is not true, however, when the nozzle is addressed normal to the surface, where at low speeds debris ejection limits the precision and cut depth. This phenomenon is not present when the electrolyte jet is inclined.

Overall this work demonstrates that using an articulated head to adjust the jet approach angle has distinct advantages which could not only increase the flexibility of the possible structures that can be created by EJP but also a simplified method for the creation of complex micro- geometries. Future investigations enabling a model to be created utilising this methodology would enable full integration into computer-aided manufacturing software enabling optimal tool-path generation for complex surface structuring by EJP.

Acknowledgments

This work was supported by the Engineering and Physical Sciences Research Council [grant numbers EP/M02072X/1, EP/L016206/1] through the “In-Jet Interferometry for Ultra Precise Electrolyte Jet Machining” project, and the EPSRC Centre for Doctoral Training in Innovative Metal Processing. The authors would like to thank The Manufacturing Metrology Team at the University of Nottingham for providing access to the metrology equipment for surface measurement, and Matthias Hirsch and Alexander Jackson-Crisp of ACEL for technical assistance with surface scanning.

References

Bocking, C.B., Dover, S..l., Bennett, G., 1995. An investigation into the suitability of high speed selective jet electrodeposition for rapid tooling. First National Conference on Rapid Prototyping and Tooling Research, MEP.

George, D.S., Onischenko, A., Holmes, A.S., 2004. On the angular dependence of focused laser ablation by nanosecond pulses in solgel and polymer materials. Appl. Phys. Lett. 84 (10), 1680–1682.

Hackert-Oschätzchen, M., Meichsner, G., Zinecker, M., Martin, A., Schubert, A., 2012. Micro machining with continuous electrolytic free jet. Precis. Eng. 36 (4), 612–619.

Hackert, M., Meichsner, G., Schubert, A., 2008. Generating micro geometries with air assisted electrochemical machining. In: EUSPEN 10th International Conference. Zurich.

Kai, S., Sai, H., Kunieda, M., Izumi, H., 2012. Study on electrolyte jet cutting. Procedia CIRP 1 (0), 627–632.

Kawanaka, T., Kato, S., Kunieda, M., Murray, J.W., Clare, A.T., 2014. Selective surface texturing using electrolyte jet machining. Procedia CIRP 13, 345–349.

Kawanaka, T., Kunieda, M., 2015. Mirror-like finishing by electrolyte jet machining. CIRP Ann.- Manuf. Technol. 64 (1), 237–240.

Kozak, J., Gulbinowicz, D., Gulbinowicz, Z., 2008. The mathematical modeling and computer simulation of pulse electrochemical micromachining. Eng. Lett. 16 (4), 556–561.

Kunieda, M., 1993. Influence of micro indents formed by electro-chemical jet machining on rolling bearing fatigue life. ASM PED 64, 693–699.

Kunieda, M., Ooshiro, S., Iwamoto, N., 2010. Manufacturing dimpled saw wires using electrolyte jet machining. J. Jpn. Soc. Precis. Eng. 76 (5), 572–576.

Mitchell-Smith, J., Clare, A.T., 2016. Electrochemical jet machining of titanium: overcoming passivation layers with ultrasonic assistance. Procedia CIRP 42, 379–383.

Mitchell-Smith, J., Murray, J.W., Clare, A.T., Kunieda, M., 2014. In: Bahre, D., Rebschlager, A. (Eds.), Electrolyte Jet Machining for Surface Texturing of Inconel 718. INSECT 2014. Saarland University, Saarbrucken, Germany, pp. 111–118.

Mitchell-Smith, J., Speidel, A., Gaskell, J., Clare, A.T., 2017. Energy distribution modulation by mechanical design for electrochemical jet processing techniques. Int. J. Mach. Tools Manuf. 122, 32–46.

Natsu, W., Ikeda, T., Kunieda, M., 2007. Generating complicated surface with electrolyte jet machining. Precis. Eng. 31 (1), 33–39.

Prakash, A., Struik, K., 1981. Roughness measurement of highly polished, mirror-finished surfaces. Precis. Eng. 3 (4), 215–219.

Rajput, M.S., Pandey, P.M., Jha, S., 2015. Modelling of high speed selective jet electrodeposition process. J. Manuf. Process. 17 (0), 98–107.

Schubert, A., Hackert-Oschätzchen, M., Martin, A., Winkler, S., Kuhn, D., Meichsner, G., Zeidler, H., Edelmann, J., 2016. Generation of complex surfaces by superimposed multi-dimensional motion in electrochemical machining. Procedia CIRP 42, 384–389.

Schubert, A., Hackert-Oschätzchen, M., Meichsner, G., Zinecker, M., 2011a. Design and realization of micro structured surfaces for thermodynamic applications. Microsyst. Technol. 17 (9), 1471–1479.

Schubert, A., Neugebauer, R., Sylla, D., Avila, M., Hackert, M., 2011b. Manufacturing of surface microstructures for improved tribological efficiency of powertrain components and forming tools. CIRP J. Manuf. Sci. Technol. 4 (2), 200–207.

Speidel, A., Lutey, A.H.A., Mitchell-Smith, J., Rance, G.A., Liverani, E., Ascari, A., Fortunato, A., Clare, A., 2016. Surface modification of mild steel using a combination of laser and electrochemical processes. Surf. Coat. Technol. 307 (Part A), 849–860.

Srinivasu, D.S., Axinte, D.A., Shipway, P.H., Folkes, J., 2009. Influence of kinematic operating parameters on kerf geometry in abrasive waterjet machining of silicon carbide ceramics. Int. J. Mach. Tools Manuf. 49 (14), 1077–1088.

Tokarev, V.N., Wilson, J.I.B., Jubber, M.G., John, P., Milne, D.K., 1995. Modelling of self-limiting laser ablation of rough surfaces: application to the polishing of diamond films. Diam. Relat. Mater. 4 (3), 169–176.

Venkatesh, V.C., 1984. Parametric studies on abrasive jet machining. CIRP Ann.- Manuf. Technol. 33 (1), 109–112.

Walker, J.C., Kamps, T.J., Lam, J.W., Mitchell-Smith, J., Clare, A.T., 2017. Tribological behaviour of an electrochemical jet machined textured Al-Si automotive cylinder liner material. Wear 376–377 (Part B), 1611–1621.

Yang, X., Liu, X., Lu, Y., Zhou, S., Gao, M., Song, J., Xu, W., 2016. Controlling the adhesion of superhydrophobic surfaces using electrolyte jet machining techniques. Sci. Rep. 6, 23985.

Yoneda, K., Kunieda, M., 1995. Processing shape simulation in the electrolytic solution jet machining. Electr. Process. J. 29 (62), 8.